Japanese Journal of Applied Physics

The Japan Society of Applied Physics

RAPID COMMUNICATION

Overcoming the excessive compressive strain in AlGaN epitaxy by introducing high Si-doping in AlN templates

To cite this article: Chia-Yen Huang *et al* 2020 *Jpn. J. Appl. Phys.* **59** 070904

View the article online for updates and enhancements.

You may also like

- Fabrication of AlN templates by high-temperature face-to-face annealing for deep UV LEDs
Kenjiro Uesugi and Hideto Miyake
- Uneven AlGaN multiple quantum well for deep-ultraviolet LEDs grown on macrosteps and impact on electroluminescence spectral output
Michiko Kaneda, Cyril Pernot, Yosuke Nagasawa et al.
- Ultraviolet-B band lasers fabricated on highly relaxed thick $Al_{0.55}Ga_{0.45}N$ films grown on various types of AlN wafers
Yuta Kawase, Syunya Ikeda, Yusuke Sakuragi et al.

This content was downloaded from IP address 140.113.78.144 on 29/03/2023 at 07:09

Japanese Journal of Applied Physics **59**, 070904 (2020) **RAPID COMMUNICATION**
https://doi.org/10.35848/1347-4065/ab990a

Overcoming the excessive compressive strain in AlGaN epitaxy by introducing high Si-doping in AlN templates

Chia-Yen Huang[1*], Sebastian Walde[2], Chia-Lung Tsai[1], Carsten Netzel[2], Hsueh-Hsing Liu[1], Sylvia Hagedorn[2], Yuh-Renn Wu[1,3], Yi-Keng Fu[1], and Markus Weyers[2]

[1]*Electronic and Optoelectronic System Research Laboratories, Industrial Technology Research Institute, 195, Sec. 4, Chung Hsing Rd., Hsinchu, 31057, Taiwan*
[2]*Ferdinand-Braun-Institut, Leibniz-Institut fuer Hoechstfrequenztechnik, Gustav-Kirchhoff-Strasse 4,12489 Berlin, Germany*
[3]*Graduate Institute of Photonics and Optoelectronics and Department of Electrical Engineering, National Taiwan University, Taipei 10617, Taiwan*

[*]E-mail: itriA70432@itri.org.tw

Received April 3, 2020; revised April 30, 2020; accepted June 2, 2020; published online June 18, 2020

The influence of compressive strain in high-quality AlN templates on the subsequent growth of AlGaN-based device layers was investigated. The AlN templates showed compressive strain of $\sim -0.29\%$ and threading dislocation densities (TDDs) below $6.5 \times 10^8\,cm^{-2}$. By introducing high Si-doping in MOVPE-grown AlN, the compressive strain was relaxed while preserving the low TDD. By this method, the low TDD was transferred from the AlN template to the micron-thick n-$Al_{0.63}Ga_{0.37}N$. A 275 nm LED was demonstrated with a $\sim$2.5 times power enhancement than the same LED on conventional MOVPE-grown AlN template under low current injection. The maximum external quantum efficiency (EQE) was enhanced from 1.6% to 2.2% with an improved n-AlGaN. © 2020 The Japan Society of Applied Physics

Al-rich (Al content >45%) AlGaN alloys have high potential for compact deep-UV (DUV) LEDs which can be used for sterilization and other biomedical applications.[1–3] Devices grown on conventional AlN templates suffer from low internal quantum efficiency (IQE) because of high threading dislocation densities (TDDs) in the AlN template.[4,5] Successive modulation of the growth condition and nano-patterned sapphire substrates (nPSS) were developed to reduce the TDD.[6–9] However, most of the high-quality AlN epitaxy on flat sapphire or nPSS showed a rather high coalescence thickness. For example, Shatalov et al. also demonstrated UVC LED with peak external quantum efficiencies (EQE) up to 10.4% on flat sapphire. To achieve a low TDD, the AlN underlayer was grown as thick as 10 μm. Takano et al. also demonstrated UVC-LEDs with EQE > 10% on nPSS.[10] The required AlN coalescence thickness is up to 8 μm.[11] Such high AlN thicknesses will bring critical challenges in wafer warpage management and uniformity improvement. The growth of bulk AlN substrates with TDD $<10^5\,cm^{-2}$ has been demonstrated.[12] Optically-pumped and electrically-pumped deep-UV lasing have been achieved on such AlN substrates.[13,14] UVC-LEDs were also demonstrated on bulk substrates, but the reported EQE is still limited to $\sim$2%.[15,16] Although AlN bulk substrates possessed a very low TDD, their limited wafer size, parasitic subband absorption, and high cost still hinders its commercial utilization for DUV LEDs. Therefore, improved AlN/sapphire templates with a high UV transparency and a decent thickness are still a goal of research. For example, Miyake et al. reduced the TDD of pre-deposited AlN buffers on flat sapphire substrates (FSS) by high-temperature (HT) annealing (>1500 °C).[17,18] AlN regrowth on the HT-annealed buffer yielded a narrow FWHM in X-ray rocking curve (RC) measurements indicating a low TDD. FWHM values of the 10–12 RC lower than 300 arcsec and AlN thickness less than 3 μm were reported by several.[19,20] However, the annealed templates are under higher compressive strain than those without HT-annealing. The compressive strain state was not only observed at room temperature, but also at growth temperature in metalorganic vapor phase epitaxy (MOVPE).[20,21] Regardless of the fabrication methods, high compressive strain is commonly observed in high-quality AlN/sapphire templates treated by a high-temperature process. Interestingly, the efforts in improving the AlN templates' material quality do not directly result in improved quality of subsequently grown AlGaN-based devices. There are rather few reports of higher device performance on such high-quality AlN templates. Susilo et al. and Itokazu et al. demonstrated deep-UV LEDs emitting at 265 nm on annealed AlN templates since the underlying AlGaN can still be coherently strained on annealed AlN templates.[22,23] However, for UV LEDs of longer wavelengths, problems with relaxation occur. Ni et al. demonstrated a $\sim$290 nm LED on an annealed template, but its peak efficiency is only 5% higher than the same LED grown on MOCVD-grown AlN templates.[24] The improvement by utilizing a high-quality template seems to be limited, which might be attributed to the limited crystal quality improvement of the thick AlGaN epitaxy above. In fact, the high compressive strain and low TDD in the template cause additional challenges for subsequent AlGaN epitaxy. In this paper, we investigate the impact of the compressive strain on subsequent AlGaN growth and show that by introducing an additional highly Si-doped AlN layer this issue can be overcome.

As a starting point three different AlN templates (A, B, C) were used. Template A was grown by MOVPE on planar sapphire at a low temperature. Templates B and C were grown by HVPE on a planar sapphire and provided by SCIOCS Co., Ltd., Japan. An additional 1.8 μm AlN was grown upon them at 1240 °C in a Taiyo-Nippon-Sanso SR-4000 MOVPE system. Trimethylaluminum (TMAl), ammonia (NH_3), and silane (SiH_4) were used as precursors. Only the 1.8 μm AlN on template C was doped with Si. According to secondary ion mass spectrometry (SIMS) measurements, the Si concentration on the AlN layer on template C was $2 \times 10^{19}\,cm^{-3}$. Figure 1 schematically illustrates the structure of all templates.

The three different templates were analyzed by high-resolution X-ray diffraction (HR-XRD) and atomic force microscopy (AFM). RC measurements were conducted for both 0002 and 10–12 reflections with an open detector. Fine-scale ω-2θ scans were conducted on the (0002) plane with a

 © 2020 The Japan Society of Applied Physics

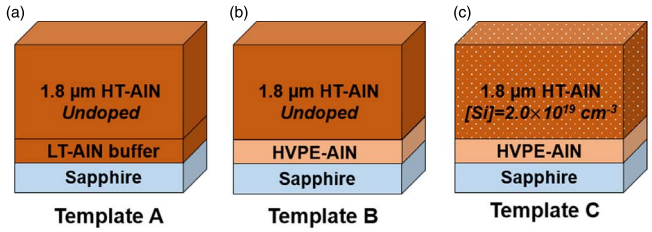

Fig. 1. (Color online) (a) to (c) Schematic structure of AlN templates A to C.

triple-axis detector. The ω-2θ scan curves are plotted in Fig. 2(a). The in-plan strain (ε_x) can be extracted by Bragg's Law and AlN's elastic constants.[25] The ε_x and measured RC FWHMs are summarized in Table I. According to the calculation, the HVPE buffer showed the narrowest RC FWHM and the highest ε_x of $-0.284\% \sim -0.298\%$ at room temperature. Although template A was also under compressive strain at room temperature ($\varepsilon_x = -0.166\%$), the strain is mostly attributed to the thermal expansion (CTE) mismatch between AlN and sapphire. Few small cracks at the edge of the wafer of template A actually indicate a slight tensile strain state at growth temperature. Therefore, the measured strain value could be misleading while estimating the strain state at growth temperature. To better assess the strain state of templates B and C at growth temperature, we define the in-plane "excess strain" (ε_x^{ex}) of template B and C by:

$$\varepsilon_x^{ex} = \varepsilon_x - \varepsilon_{x,A}, \tag{1}$$

$\varepsilon_{x,A}$ refers to the in-plane strain of template A at room temperature. Since all templates experienced the same cooling process in MOVPE, the common thermal strain contribution can be subtracted by evaluating the excess strain. For template B, there is no discernible peak splitting in the ω-2θ scan. We assume that the MOVPE-AlN was grown nearly coherent on the HVPE buffer. ε_x^{ex} was estimated to be -0.132% for both HVPE template and regrown AlN, which is equivalent to the strain of $Al_{0.95}Ga_{0.05}N$ coherently grown on freestanding AlN. For

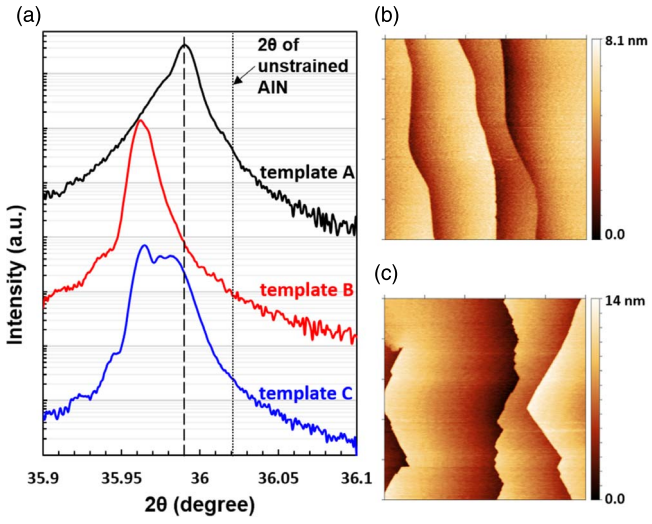

Fig. 2. (Color online) (a) Fine-scale 0002 ω-2θ scan of templates A to C. The curves were vertically shifted. The dotted line represents the 2θ for unstrained AlN. The dashed line marks the peak 2θ position of template A for reference. 5 μm × 5 μm AFM images of (b) template B and (c) template C.

template C, a clear peak splitting in the ω-2θ scan was observed. This is attributed to a relaxation of the Si-doped AlN on the HVPE template resulting in a reduction of ε_x^{ex} from -0.118% to -0.034%. Although the final strain state of template C was close to template A, the wafer appeared to be crack-free. It might be explained by that the AlN was still in compressive strain during the most of growth time. According to Lee's model, the TDD with edge or screw component can be estimated from RC FWHMs.[26] The modeled TDDs are also summarized in Table I. The TDDs with edge component in template B and C were estimated to be $<6.5 \times 10^8\,m^{-2}$, which was around one-fifth of that in template A. The TDD with a screw component were similar and about one order lower than for those with edge component.

Since the atomic size of Si is close to Al and its amount is in the doping level range, it is unlikely that the atom size mismatch drove the strain relaxation. According to first principle calculations, Si-doping in AlN is strongly compensated by Al vacancies (V_{Al}), which yield a very low free carrier density in n-type AlN.[27] However, from the perspective of crystal growth, the effective incorporation of III-vacancies promotes surface-mediated dislocation inclination.[28–30] If an Al vacancy is captured by the core of a dislocation with edge component, an atomistic-level "jog" occurs on the extra half-plane. As the jogs accumulate during growth, the local compressive strain eventually relaxes as the extra half-plane gradually recedes. Similar phenomena were observed in n-GaN on UID-GaN, but the effect in n-GaN is less prominent. According to Xie et al., peak separation between n-GaN and UID-GaN in XRD ω-2θ scan is observed only if the TDD is sufficiently high ($TDD > 10^9\,cm^{-2}$).[31] N-GaN layers with TDD $\sim 3 \times 10^8\,cm^{-2}$ did not exhibit any discernible peak separation even with a [Si] $\sim 2 \times 10^{19}\,cm^{-3}$. Additionally, the surface morphology of n-GaN did not change for Si concentrations up to $2.5 \times 10^{19}\,cm^{-3}$. But in this report, Si-doping in AlN was accompanied by morphological changes. In Figs. 2(b) and 2(c), macrosteps can be seen on the surface aligning as smooth curves on template B. After introduction of Si-doping in template C, the terrace shape of the macrosteps turns into zig-zag lines with an angle of 120 degree. Most probably, the vacancies were not only captured by the dislocations, but also by the macrosteps. As a result, growth pinning occurs at the vacancy sites, leading to faceting of the macrostep growth front.

In order to investigate the impact of the template's high initial strain and its TDD on device epitaxy, we grew identical 1.8 μm thick AlGaN layers on top of the MOVPE-grown AlN layers at T = 1050 °C. The AlGaN consisted of a 150 nm compositional-graded layer followed by 1.5 μm n-$Al_{0.63}Ga_{0.37}N$ and 150 nm n^+-$Al_{0.58}Ga_{0.42}N$. This structure is our typical underlayer for ~275 nm UVC-LEDs. The AlGaN samples are named according to the used template Y as AlGaN-Y (Y = A, B, or C), and they were analyzed by skew-symmetric (11–24) plane reciprocal space mapping (RSM) by HR-XRD. RSM of all AlGaN samples and their schematic structure are plotted in Fig. 3. The in-plane lattice constant of a particular layer L (a_L, L = AlN or AlGaN) can be extracted by its $Q_{x,L}$ coordinates. In the beginning of AlGaN growth, the AlGaN is coherently

© 2020 The Japan Society of Applied Physics

Table I. Summary of 0002 and 10–12 RC FWHM's of templates before and after MOVPE regrowth and their extracted in- plane strain from Fig. 2(a).* The strain states of template B and C is only measured after regrowth. Since the AlN peaks in template B are indistinguishable. In-plain strain of both the HVPE buffer and regrown AlN has been assigned the same value.

Template		RC FWHM (arcsec)				TDD (cm^{-2})	
		0002	10–12	ε_x (%)	ε_x^{ex} (%)	edge + mixed	screw + mixed
A	After growth	150	530	−0.166		3.2×10^9	4.8×10^7
B	HVPE buffer	82	279	−0.298*	−0.132*	8.8×10^8	1.4×10^7
	After regrowth	148	258			6.5×10^8	4.6×10^7
C	HVPE buffer	73	260	−0.284	−0.118	7.7×10^8	1.1×10^7
	After regrowth	149	239	−0.200	−0.034	5.5×10^8	4.7×10^7

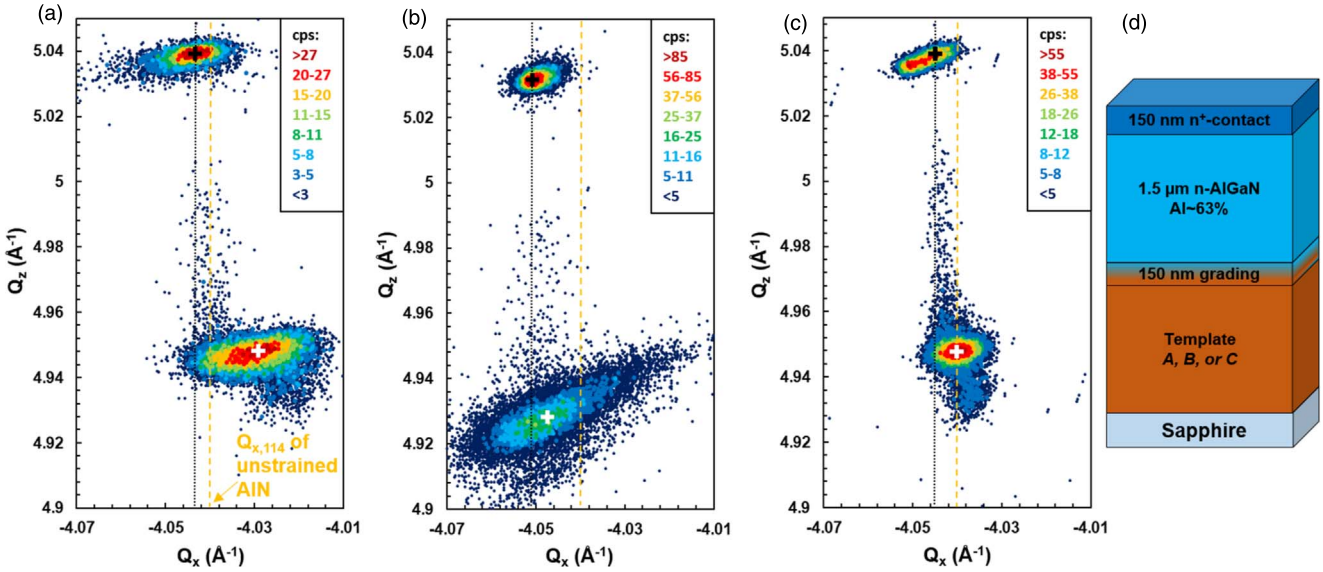

Fig. 3. (Color online) Reciprocal space maps of the 11–24 reflection of (a) AlGaN-A, (b) AlGaN-B and (c) AlGaN-C. The yellow dashed lines and black dotted lines represent the Q_x coordinates of unstrained AlN and measured AlN templates, respectively. The black and white crosses mark the AlN and AlGaN peaks. The schematic structure of the AlGaN samples is shown in (d).

strained on its AlN template. Therefore, the initial strain of AlGaN ($\varepsilon^i_{\mathrm{AlGaN}}$) is:

$$\varepsilon^i_{\mathrm{AlGaN}} = (a_{\mathrm{AlN}} - a^0_{\mathrm{AlGaN}})/a^o_{\mathrm{AlGaN}}. \quad (2)$$

a^o_{AlGaN} is the lattice constant of freestanding $Al_{0.63}Ga_{0.37}N$ according to Vegard's law. During growth, the lattice constant relaxes to the determined AlGaN peak in the RSM. The AlGaN strain relaxation (f_{AlGaN}) can be defined as:

$$f_{\mathrm{AlGaN}} = (a_{\mathrm{AlGaN}} - a_{\mathrm{AlN}})/a^o_{\mathrm{AlGaN}}. \quad (3)$$

The extracted a_{AlN}, a_{AlGaN} and their strain statuses are summarized in Table II.

According to Table I, AlN FWHM's of AlGaN-B and AlGaN-C were both narrow. However, the AlGaN peak width differed significantly between AlGaN-B and AlGaN-C in the RSM. A narrower AlGaN peak is only preserved in AlGaN-C. The measured 10–12 RC FWHM of the $Al_{0.63}Ga_{0.37}N$ layer was 490 arcsec, 740 arcsec, and 306 arcsec for AlGaN-A, AlGaN-B and AlGaN-C, respectively. According to the same model, the TDD of AlGaN was estimated to be $2.6 \times 10^9\,cm^{-2}$, $6.7 \times 10^9\,cm^{-2}$, and $8.5 \times 10^8\,cm^{-2}$, for AlGaN-A –B and –C, respectively. Therefore, directly transferring the same AlGaN growth process from one AlN buffer to another one with a lower TDD does not necessarily result in an improvement of the final AlGaN quality if the strain is not properly managed.

Table II. Extracted lattice constants, initial strain ($\varepsilon^i_{\mathrm{AlGaN}}$), strain relaxation ($f_{\mathrm{AlGaN}}$), and the 10–12 RC FWHM of AlGaN.

AlGaN–	a_{AlN} (Å)	a_{AlGaN} (Å)	$\varepsilon^i_{\mathrm{AlGaN}}$ (%)	f_{AlGaN} (%)	10–12 RC FWHM (arcsec)
A	3.108	3.118	−1.02	0.31	490
B	3.102	3.105	−1.20	0.09	743
C	3.107	3.111	−1.04	0.12	306

The strain energy of AlGaN can be relaxed via TD inclination or misfit dislocation (MD) formation through pre-existing TDs.[32] Therefore, f_{AlGaN} of AlGaN-A appears to be highest. Relaxation via existing TDs is preferable because the overall TDD will not increase. However, the relaxation can also be through new TD nucleation during growth. The activation energy of TD nucleation is higher and the final TDD in the epilayer will dramatically increase. Thus it will only be active if the pre-existing TDs fail to accommodate the accumulating strain energy. New TD nucleation was rarely discussed in the AlGaN/AlN system because the pre-existing TDD is usually very high. Therefore, the compressive strain can mostly effectively relaxed by existing TDs. New TD nucleation is more commonly observed in the InGaAs/GaAs system, for which the initial TDD is very low and the lattice-mismatch between the epitaxial layer and substrate is significant.[33] In this report,

© 2020 The Japan Society of Applied Physics

TD nucleation in AlGaN can take place due to the low TDD and high compressive strain of the AlN buffer. The measured ε^{i}_{AlGaN} of AlGaN-A, AlGaN-B, and AlGaN-C was −1.02%, −1.20%, and −1.04%, respectively. Although the measured strain still partly stems from the AlGaN/sapphire CTE mismatch, this effect is not dominant during growth. For example, the theoretical lattice strain of $Al_{0.63}Ga_{0.37}N$ coherent on freestanding AlN at room temperature is −0.92%, which is −0.1% less than the AlGaN-A case. Therefore, we preliminarily assumed an −0.1% contribution of thermal strain without loss of generality. After subtracting the thermal strain, the initial lattice strain of AlGaN-B was ∼20% higher than that of others during AlGaN growth. Since the strain energy goes with the square of the in-plane strain, the strain energy in AlGaN-B accumulated >40% faster than the others. As a result, new TD nucleation was activated in AlGaN-B first during AlGaN growth. If multi-quantum-wells (MQWs) are grown on AlGaN-B, the strain-induced defects would further propagate and multiply because of an even higher lattice-mismatch. Therefore, further growth of a full LED heterostructure upon AlGaN-B would lead to very limited device performance.

To verify the device performance on a high-quality AlN template, the same UVC LED layer structure was grown on AlGaN-A and AlGaN-C. The LED heterostructure consisted of a fourfold AlGaN MQW, a 40 nm thick p-type $Al_{0.75}Ga_{0.25}N$ electron-blocking layer, and 80 nm p-GaN. 1 mm × 1 m flip-chips were fabricated with conventional processing technologies. The p-electrode was indium-tin oxide (ITO) and the n-electrode was a Ti/Al/Ni/Au metal multilayer. The chips were bonded on TO-cans and tested in an integrating sphere without encapsulation. The electroluminescence (EL) spectra and external quantum efficiency (EQE) curves with injection current of selected chips are plotted in Fig. 4. The absolute EQE is still rather limited (maximum EQE ∼ 2.2%) due to the strong band-edge absorption from p-GaN and ITO and lack of other light-extraction designs. The enhancement of EQE is more significant under low current injection. The enhancement factor is up to 2.5 at I = 10 mA, while it is 1.25 at I = 350 mA. The strong improvement at lower current can be attributed to the suppressed non-radiative recombination because of a lower TDD in the MQW on AlGaN-C. If the TDD of MQW is close to that from AlGaN-A and AlGaN-C, we might roughly assess LEDs' internal quantum efficiency (IQE) from the theoretical model in Ref. 5. Under a low excitation (carrier density $\sim 1 \times 10^{18}\,cm^{-3}$), the IQE was estimated to be 9% and 24% for LED on AlGaN-A and AlGaN-C, respectively. The magnitude of IQE improvement is consistent with the LED EQE enhancement under low current injection. As the injection current increases, carrier overflow effect eventually dominates the performance instead. Therefore, the output power enhancement became less significant.

In conclusion, we revealed the inherent difficulty of fabricating UVC-LEDs on high-quality AlN/sapphire templates with low TDD but high compressive strain. Although a high-quality AlN layer can be regrown easily, the growth of subsequent AlGaN epilayers becomes much more challenging. Both the high compressive strain and reduced TDD lead to relaxation during growth of the lattice-mismatched

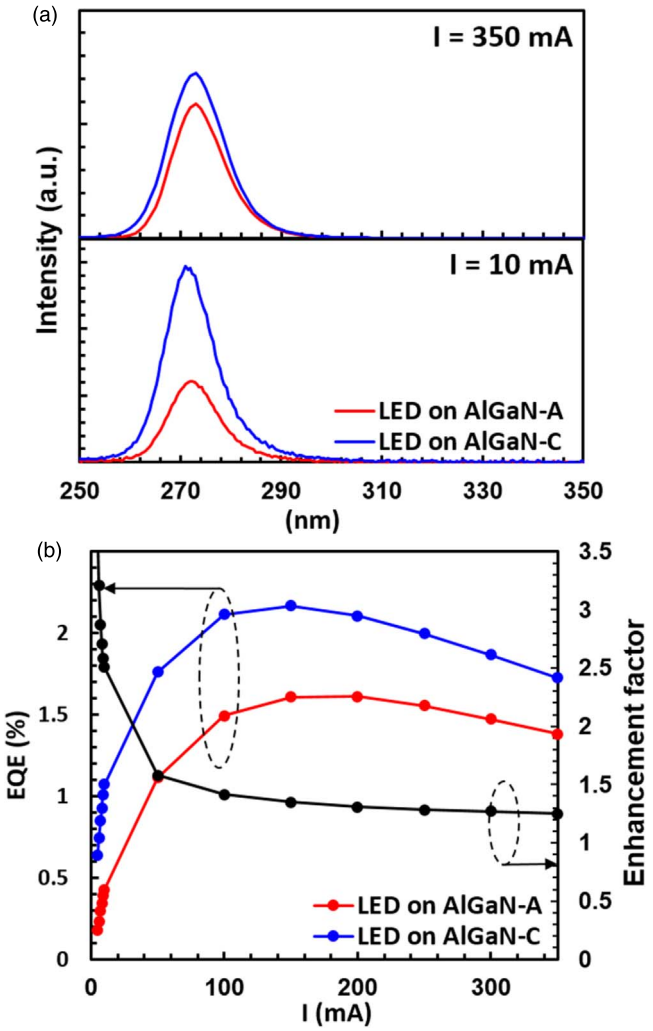

Fig. 4. (Color online) (a) EL spectra of LEDs on AlGaN-A or AlGaN-C under 10 mA (lower) and 350 mA (upper) (b) EQE-I curves and enhancement factor of selected LEDs.

AlGaN resulting in nucleation of new defects. As a result, high-quality AlGaN can only be grown with a reduced Ga content or a limited thickness. This might not fit the original device functionality requirement. Since a low TDD is still desired, relaxing the inherent compressive strain is desirable. Thanks to the strong self-compensation effect in AlN, introducing Si-doping effectively relaxed the lattice by vacancy-mediated dislocation inclination even with a relatively low TDD. The combination of high-quality HVPE AlN buffers and Si-doping in the regrown AlN paves the way for high-performance and cost-effective AlGaN-based devices.

This work was partially funded by the German Federal Ministry of Education and Research (BMBF) within the Advanced UV for Life consortium and by the German Research Foundation (DFG) within the Collaborative Research Center "Semiconductor Nanophotonics" (CRC 787). This work was also partially funded by Ministry of Science and Technology, Taiwan under the contact number MOST 108-2628-E-002-010-MY3.

ORCID iDs Chia-Yen Huang https://orcid.org/0000-0003-0844-1903

© 2020 The Japan Society of Applied Physics

1) M. Kneissl and J. Rass, "III-Nitride ultraviolet emitters," *Springer Series Material Science* (Springer, Berlin, 2016).
2) H. Hirayama, T. Yatabe, N. Noguchi, and N. Kamata, Electron. Commun. Jpn. **93**, 24 (2010).
3) M. Kneissl, T.-Y. Seong, J. Han, and H. Amano, Nat. Photonics **13**, 233 (2019).
4) J. Mickevicius, G. Tamulaitis, M. Shur, M. Shatalov, J. Yang, and R. Gaska, Appl. Phys. Lett. **101**, 211902 (2012).
5) K. Ban, J. Yamamoto, K. Takeda, K. Ide, M. Iwaya, T. Takeuchi, S. Kamiyama, I. Akasaki, and H. Amano, Appl. Phys. Express **4**, 052101 (2011).
6) J. Bai, M. Dudley, W. H. Sun, H. M. Wang, and M. A. Khan, , Appl. Phys. Lett. **88**, 051903 (2006).
7) P. Dong et al., J. Cryst. Growth **395**, 9 (2014).
8) L. Zhang et al., Sci. Rep. **6**, 35934 (2016).
9) Y. Iba, K. Shojiki, K. Uesugi, S. Xiao, and H. Miyake, J. Cryst. Growth **532**, 125397 (2020).
10) M. Shatalov et al., Appl. Phys. Express **5**, 082101 (2012).
11) T. Takano, T. Mino, J. Sakai, N. Noguchi, K. Tsubaki, and H. Hirayama, Appl. Phys. Express **10**, 031002 (2017).
12) Y. Kumagai et al., Appl. Phys. Express **5**, 055504 (2012).
13) R. Kirste, Q. Guo, J. H. Dycus, A. Franke, S. Mita, B. Sarkar, P. Reddy, J. M. LeBeau, R. Collazo, and Z. Sitar, Appl. Phys. Express **11**, 082101 (2018).
14) Z. Zhang, M. Kushimoto, T. Sakai, N. Sugiyama, L. J. Schowalter, C. Sasaoka, and H. Amano, Appl. Phys. Express **12**, 124003 (2019).
15) J. R. Grandusky, S. R. Gibb, M. C. Mendrick, C. Moe, M. Wraback, and L. J. Schowalter, Appl. Phys. Express **4**, 082101 (2011).
16) T. Kinoshita, T. Obata, T. Nagashima, H. Yanagi, B. Moody, S. Mita, S. Inoue, Y. Kumagai, A. Koukitu, and Z. Sitar, Appl. Phys. Express **6**, 092103 (2013).
17) H. Miyake, C.-H. Lin, K. Tokoro, and K. Hiramatsu, J. Cryst. Growth **456**, 155 (2016).
18) R. Yoshizawa, H. Miyake, and K. Hiramatsu, J. Jpn. Appl. Phys. **57**, 01AD05 (2018).
19) C. Y. Huang et al., AIP Adv. **7**, 055110 (2017).
20) S. Walde, S. Hagedorn, and M. Weyers, J. Jpn. Appl. Phys. **58**, SC1002 (2019).
21) M. X. Wang et al., Appl. Phys. Lett. **114**, 112105 (2019).
22) N. Susilo et al., Appl. Phys. Lett. **112**, 041110 (2018).
23) Y. Itokazu, S. Kuwaba, M. Jo, N. Kamata, and H. Hirayama, J. Jpn. Appl. Phys. **58**, SC1056 (2019).
24) R. Ni, C. C. Chuo, K. Yang, Y. Ai, L. Zhang, Z. Cheng, Z. Liu, L. Jia, and Y. Zhang, J. Alloy Compd. **794**, 8 (2019).
25) I. Vurgaftman and J. R. Meyer, J. Appl. Phys. **94**, 3675 (2003).
26) S. R. Lee, A. M. West, A. A. Allerman, K. E. Waldrip, D. M. Follstaedt, P. P. Provencio, D. D. Koleske, and C. R. Abernathy, Appl. Phys. Lett. **86**, 241904 (2005).
27) J. S. Harris, J. N. Baker, B. E. Gaddy, I. Bryan, Z. Bryan, K. J. Mirrielees, P. Reddy, R. Collazo, Z. Sitar, and D. L. Irving, Appl. Phys. Lett. **112**, 152101 (2018).
28) A. Mogilatenko, A. Knauer, U. Zeimer, C. Hartmann, H. Oppermann, and M. Weyers, J. Cryst. Growth **462**, 18 (2017).
29) D. M. Follstaedt, S. R. Lee, A. A. Allerman, and J. A. Floro, J. Appl. Phys. **105**, 083507 (2009).
30) S. Fritze, A. Dadgar, H. Witte, M. Bugler, A. Rohrbeck, J. Blasing, A. Hoffmann, and A. Krost, Appl. Phys. Lett. **100**, 122104 (2012).
31) J. Xie, S. Mita, A. Rice, J. Tweedie, L. Hussey, R. Collazo, and Z. Sitar, Appl. Phys. Lett. **98**, 202101 (2012).
32) Z. Wu, K. Nonaka, Y. Kawai, T. Asai, F. A. Ponce, C. Chen, M. Iwaya, S. Kamiyama, H. Amano, and I. Akasaki, Appl. Phys. Express **3**, 111003 (2010).
33) C. Lynch, E. Chason, and R. Beresford, J. Appl. Phys. **100**, 013525 (2006).

© 2020 The Japan Society of Applied Physics